frontiers | Frontiers in Nanotechnology

TYPE Mini Review
PUBLISHED 15 January 2026
DOI 10.3389/fnano.2025.1667217

OPEN ACCESS

EDITED BY
Chiara Trovatello,
Columbia University, United States

REVIEWED BY
Jacopo Stefano Pelli Cresi,
Luxottica Group SpA, Italy

*CORRESPONDENCE
Christoph Gadermaier,
christoph.gadermaier@polimi.it

RECEIVED 16 July 2025
REVISED 02 December 2025
ACCEPTED 18 December 2025
PUBLISHED 15 January 2026

CITATION
Gadermaier C (2026) High-harmonic generation in two-dimensional semiconductors.
Front. Nanotechnol. 7:1667217.
doi: 10.3389/fnano.2025.1667217

High-harmonic generation in two-dimensional semiconductors

Christoph Gadermaier*

Dipartimento di Fisica, Politecnico di Milano Piazza Leonardo da Vinci 32, Milano, Italy

High-harmonic generation has been established in gases both as a source of extreme ultraviolet light as well as a tool for studying atomic and molecular physics in the attosecond time domain. The more recent extension of these methods to condensed matter affords much higher conversion efficiencies and offers an even richer selection of accessible phenomena. Atomically thin two-dimensional semiconductors combine mechanical robustness with intriguing many-body physics and exceptionally strong light-matter interaction. This mini-review gives a glance into the high-harmonic generation mechanisms in two-dimensional semiconductors, with particular emphasis on symmetry considerations, many-body effects, photodoping, and techniques to further enhance the high-harmonic generation efficiency.

KEYWORDS

all-optical modulation, attosecond spectroscopy, berry curvature, excitons, high harmonic generation, many-body physics, MoS_2, two-dimensional semiconductors

1 Introduction

High-order harmonic generation (HHG) is the foundation of Attosecond Science (Antoine et al., 1996; Corkum and Krausz, 2007; Calegari et al., 2007). The non-linear interaction of a strong laser field with matter drives the electron motion, emitting radiation extending up to the extreme ultraviolet domain. The resulting train of attosecond bursts can be used as a tabletop attosecond radiation source (Sansone et al., 2006). Moreover, the HHG spectrum encodes a direct fingerprint of a material's electronic structure (Vozzi et al., 2011) and its changes triggered by the laser on the attosecond timescale.

The electronic and atomic dynamics following the excitation are connected to the relaxation of a highly excited state through several decay channels like multi-electron-hole excitations, collective modes, phonon excitations, charge transfer, and even formation or breaking of chemical bonds and molecular rearrangements (Baker et al., 2006; Smirnova et al., 2009; Bruner et al., 2016). These microscopic mechanisms, which take place on extremely short timescales, are the basis for numerous potential applications, from solar energy harvesting to nanotechnology, biochemistry and life science.

The recent shift of laser technology towards the realization of few-cycle strong laser pulses in the mid-infrared regime (Vozzi et al., 2006; Vozzi et al., 2007) has enabled HHG from bulk crystals (Ghimire et al., 2011), which naturally holds a series of advantageous features, such as a compact configuration to simplify the operation conditions, the requirement of lower pulse intensities (few μJ in solids vs. few mJ in gases) (Lanin et al., 2017; Li et al., 2020), and the involvement of strong electron interactions (Ghimire and Reis, 2019). This opened new perspectives for probing the electron dynamics in solids (Silva et al., 2018) and for generating extreme ultraviolet laser sources with high efficiency (Luu et al., 2015; Garg et al., 2018).

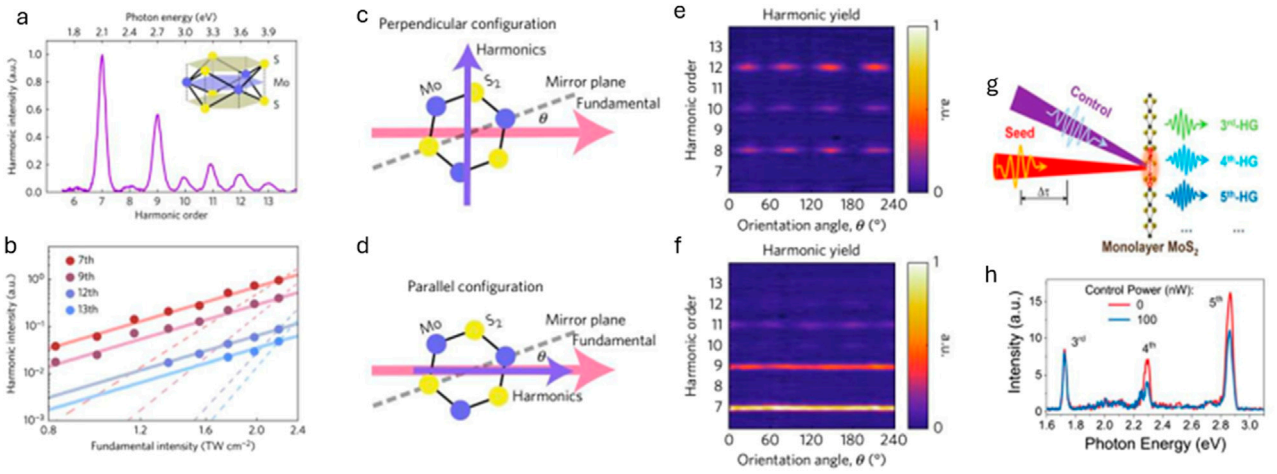

FIGURE 1
(a) HHG spectrum from monolayer MoS_2. The spectrum shows the sixth to the 13th harmonics of the driving light centered at a photon energy of 0.30 eV. The inset illustrates the crystal structure of the MoS_2 monolayer. **(b)** Harmonic intensity from monolayer MoS_2 as a function of the peak pump intensity I for representative harmonic orders n = 7, 9, 12 and 13 (dots). A fit of the experimental data to a power law, I^p, yields a phenomenological exponent of p = 3.3 for all four harmonic orders (solid lines). This behavior deviates strongly from the behavior for a perturbative nonlinear response of I^n (dashed lines, scaled to experiment at the highest intensity). **(c,d)** Dependence of HHG on crystallographic orientation of monolayer MoS_2. Experimental arrangement of HHG for detection polarized perpendicular **(c)** and parallel **(d)** to the driving field. The red and blue arrows represent the electric field polarization direction of the driving and generated light, respectively. The dashed line identifies the (perpendicular) mirror symmetry plane of the crystal, and θ denotes the relative angle between the mirror plane and the fundamental field. **(e, f)** False color representation of the HHG spectrum versus crystal orientation in the perpendicular **(e)** and parallel **(f)** polarization configuration. The color bar represents the measured harmonic yield on a linear scale. **(g,h)** All-optical control of HHG. **(g)** Schematic illustration of optically controlled HHG in monolayer MoS_2. HHG produced by excitation with the driving (seed) light in monolayer MoS_2 is modulated via exposure to the control pulse preceding the seed pulse. **(h)** HHG spectra revealing the intensity associated with third, fourth, and fifth harmonics in the presence (blue) and absence (red) of the control light. The photon energy of control light is ~3.1 eV with an average power of ~100 nW (corresponding peak intensity $I_c \sim 1.44$ GW/cm^2), and the seed light photon energy is ~0.57 eV with an average power of ~80 μW (corresponding peak intensity $I_0 \sim 1.15$ TW/cm^2). The time delay $\Delta\tau$ between the control and seed light pulses is ~0.4 ps. Reproduced with permission from (Liu et al., 2017) **(a–f)** and (Wang et al., 2022) **(g,h)**.

The laser-driven control of ultrafast electronic processes allows manipulating the non-linear current in a solid, which can be the first step towards petahertz optoelectronic devices (Schiffrin et al., 2013; Schultze et al., 2013; Krausz and Stockman, 2014). Furthermore, HHG spectroscopy enables access to the physical properties of a solid in an all-optical way, allowing the reconstruction of the band-structure and its out-of equilibrium evolution (Vampa et al., 2015a; Lanin et al., 2017).

2 Basics of the HHG mechanism

In the gas phase, HHG is widely understood within a semiclassical three-step model: an electron tunnels into the free-electron continuum, where it is accelerated and eventually emits a high-energy photon when it recombines with a bound hole (Vampa et al., 2014; Lee et al., 2024). In solids, electron–hole wave packets are promoted to conduction and valence bands via quantum tunneling. The duration of the tunneling excitation window is typically few hundreds of attoseconds to single femtoseconds, depending on the frequency of the driving light. Subsequently, the carriers are coherently accelerated in the crystal by the oscillating field and propagate far from their equilibrium positions. The electron and hole can eventually recombine, generating high energy photons via the interband mechanism of HHG (Vampa et al., 2014; Vampa et al., 2015b; Ghimire and Reis, 2019; Yoshikawa et al., 2019). Due to the nonparabolicity of electron and hole dispersion in the material, the harmonically driven carriers undergo anharmonic motion (Golde et al., 2008; Schubert et al., 2014; Wu et al., 2015), resulting in additional sources of nonlinear current due to Bloch oscillations and anomalous velocities associated with the Berry curvature of the bands (Ghimire et al., 2011; Vampa et al., 2014; Ghimire and Reis, 2019; Lee et al., 2024) in what is known as the intraband mechanism of HHG. Both inter- and intraband transitions play decisive roles for solid-state HHG. Their complex interplay can either enhance or counteract the HHG efficiency. A deeper understanding of its intricacies holds the promise for achieving higher HHG efficiencies and for identifying control parameters to manipulate HHG efficiency and spectra.

3 Two-dimensional semiconductors

Two-dimensional semiconductors, in particular transition metal dichalcogenides (TMDs) such as MoS_2 (see the inset of Figure 1a), combine mechanical and photochemical robustness with multifaceted exciton and higher many-body physics, valley degree of freedom, and exceptionally strong light-matter interaction. Monolayers (MLs) of TMDs with sub-nm thickness exhibit a wide gamut of photonic functionalities, including photodetection (Yin et al., 2012), photovoltaics (Fontana et al., 2013), saturable

absorption (Zhang et al., 2014), optical gain (Ye et al., 2015), photocatalysis (Peng et al., 2016), electrooptical modulation (Vella et al., 2017), and optical parametric amplification (Trovatello et al., 2021).

Bulk MoS_2 is built from layers consisting of a sheet of Mo atoms and two hexagonal lattices of S atoms in trigonal prismatic arrangement. The layers are stacked in 2H order, with pairs of layers forming a repeat unit. Unlike the bulk, the 1H monolayer breaks inversion symmetry. In addition to the semiconducting 2H (1H) phase, a metallic octahedral 1T phase arises upon strong doping, e.g. using Li intercalation (Joensen et al., 1986; Sandoval et al., 1991). ML TMDs have a hexagonal Brillouin zone similar to graphene, but due to the lack of inversion symmetry it has inequivalent K and K′ valleys (conduction band minima and valence band maxima) at the corners (Xiao et al., 2012; Schaibley et al., 2016). These valleys can be represented by a pseudospin 1/2. Carriers in the K and K′ valleys are subject to Berry curvatures of the same magnitude but opposite sign (Feng et al., 2012), which act like effective magnetic fields in momentum space. The strong spin-orbit coupling together with the time-reversal symmetry causes spin splitting with opposite signs at the K and K′ valleys, thus coupling the spin and valley pseudospin (Xiao et al., 2012). Composite quasiparticles, such as excitons, bear a valley polarization due to the valley localization of their constituent electrons and holes, resulting in a valley dependent optical selection rule, in which right and left circularly polarized light couples to inter-band transitions at opposite valleys.

In the linear regime, the most prominent optical feature of many-body physics in ML TMDs are strong excitonic resonances in the absorption spectrum even at room temperature. These are enabled by large effective masses and a low dielectric screening of the Coulomb interaction. Exciton binding energies are of the order of hundreds of meV and MLs of sub-nm thickness absorb up to 10%–20% of the incident light at the excitonic resonances (Chernikov et al., 2014; He et al., 2014). This unusually strong light-matter interaction can be further enhanced using external resonator structures such as distributed Bragg reflectors (Chen et al., 2018). The strongly bound, room-temperature stable excitons determine key optoelectronic properties and form the basis for yet more complex many-body quasiparticles, such as trions or biexcitons. Importantly, Coulomb correlations can be sensitively tuned by stacking monolayers; the exciton binding energy is strongly reduced in multilayer TMD crystals (Evans and Young, 1967). Photoexcitation with excess energy with respect to the lowest exciton resonance generates hot electron-hole pairs, which relax to form a mixed population of excitons and free carriers (leading to photodoping) on a few-hundred fs timescale. Such population subsequently recombines with typical time constants of tens to hundreds of ps (Borzda et al., 2015; Vega-Mayoral et al., 2016; Trovatello et al., 2022).

Atomically thin semiconductors have the distinct advantage that propagation effects such as phase matching and reabsorption of the generated high harmonics are minimized. The seminal work on HHG in ML MoS_2 by (Liu et al., 2017) found a pump intensity dependence of $I^{3.3}$ for all observed even and odd harmonics (Figures 1a, b). Since in the perturbative limit we would expect the nth harmonic yield to scale as I^n, this result establishes the non-perturbative character of the generation process.

4 Symmetry considerations

HHG in solids depends crucially on crystal symmetry. In multilayer MoS_2, different HHG patterns have been found for different crystalline polytypes, highlighting the role of crystal structure in the HHG process and the scope of using the details of the HHG spectrum and its angular dependence as a fingerprint of a material's structural properties (Jia et al., 2020). The effect of broken inversion symmetry in ML TMDs is observed as the emission of even-order harmonics (Liu et al., 2017; Yoshikawa et al., 2019; Lou et al., 2020; Liu et al., 2020; Cao et al., 2021) (Figures 1a, e, f). Berry curvature acts as a pseudomagnetic field and drives anomalous currents perpendicular to the electric field of the pump laser. The contributions of intraband motion in the K and K′ cancel for the driving field component along a mirror plane, but not for the perpendicular component.

An anisotropy study of HHG in WS_2 and $MoSe_2$ found contrasting results for the two materials (Kobayashi et al., 2021). In WS_2, the polarization of the odd-order harmonics continuously follows the direction of the driving laser field (Figure 1d), whereas the even-order harmonics are polarized parallel to the crystal mirror planes. A sudden flip of the polarization of the even-order harmonics from one crystal mirror plane to another occurs as the laser polarization direction (angle β in Figures 1c, d) is about midway between the two mirror planes. In $MoSe_2$, a deviation from these trends indicates that the symmetry effects are material dependent and suggests that polarization-resolved HHG measurements can reveal the roles of the intra- and interband contributions as well as the deflection of the electron-hole trajectories by nonparabolic bands in the crystal (Kobayashi et al., 2021).

In ML MoS_2, HHG as a function of crystal orientation relative to the pump light polarization (angle β in Figures 1c, d) shows pronounced nodes in the HHG spectra at certain crystal orientations (Yue et al., 2022). In addition, for several mid-infrared wavelengths, the parallel-polarized odd-order harmonics below (above) 3.5 eV are enhanced for driver polarization along the armchair (zigzag) direction, which can be traced to electron-hole recombination from different conduction bands, effectively probing the vectorial nature of recombination dipoles in different bands (Yue et al., 2022).

5 Many-body effects

In ML TMDs, the electric field uniting an electron and a hole into an exciton is of comparable magnitude to that of the light driving the HHG. Indications for the potential importance of Coulomb correlations in this regime in ML TMDs were first reported in (Liu et al., 2017), who found a significantly higher HHG efficiency for ML vs. bulk MoS_2. This was attributed to the more efficient screening of the driving field in the bulk case. Similarly, high-order sideband generation in bulk and ML WSe_2 (Freudenstein et al., 2022) found significant influence of Coulomb correlations. A pump-probe experiment on ML WS_2 using a sub-resonant infrared pump as typically used for HHG showed that even at the critical field strength for ionization, the exciton develops a Floquet sideband but remains intact (Kobayashi et al., 2023).

Coulomb correlations are expected to dramatically enhance the HHG (Hader et al., 2023). For sub-resonant pump energies up to approximately the exciton binding energy, the coupling to and between excitonic states with high oscillator strength leads to an increase of HHG intensities of up to approximately two orders of magnitude. The enhancement becomes weaker for higher excitation energies. For excitation near and above the bound excitonic states the enhancement is reduced to a factor of approximately two to three. Here, strong absorption leads to bleaching of the absorption and pinning of the distributions near half-filled level. This leads to a broad emission sub-floor for each harmonic (Hader et al., 2023).

Many-body interactions are key to capturing the relative strength of harmonics in the direction perpendicular to the driving field, while harmonics parallel to the driving field remain qualitatively similar to the non-interacting independent particle picture (Lee et al., 2024). The importance of many-body effects in the perpendicular configuration is a consequence of the interplay of an excitonic enhancement of the oscillator strength for interband transitions together with the anomalous intraband velocity arising from the Berry curvature, which can drive the electron and hole in the same direction in real space, leading to the potential for enhanced electron-hole correlation effects. In addition to the A and B excitons at the K and K′ points in the Brillouin zone, also the C and D resonances originating from band nesting enhance the HHG (Yoshikawa et al., 2019).

6 Photodoping

All-optical control of HHG (Guan et al., 2020) is realized by exciting the carriers with a resonant control pulse prior to the impact of the strong infrared pulse that drives the HHG (Figures 1g, h), achieving a high modulation depth of ~95% in ML MoS_2 at a control pulse energy of 250 pJ (Wang et al., 2022). The control pulse redistributes valence band carriers to the conduction band, which decreases the HHG efficiency within 100 fs or less. Subsequently, HHG starts recovering with two different time constants along with the relaxation of photocarriers. The faster time constant of the order 1 ps can be understood as the result of carrier relaxation processes, while the slow time constant of the order 100 ps should be associated with slower electron-hole recombination processes (Borzda et al., 2015; Vega-Mayoral et al., 2016; Trovatello et al., 2022). The high modulation depth of the fourth and fifth harmonic generation by as much as 95% (84%) suggests that interband polarization contributes dominantly to HHG in the explored energy region.

The decrease in the HHG yield induced by the control pulse (Figures 1g, h), to a large extent arises from dephasing of the coherent electron–hole wave packets (Heide et al., 2022; Peterka et al., 2023), rather than solely from a weakening of the interband transition by simple phase-space filling. The generated high harmonic radiation results from the macroscopic nonlinear current of coherently oscillating electrons. Once the quantum phase between the electron and the field of the driving infrared wave is lost, the electron does not further contribute to the generated coherent wave. The most important scattering processes are electron–phonon scattering, electron–electron scattering, and scattering at ionized impurities. While the electron–phonon scattering times for electrons with low kinetic energy are typically long (hundreds of femtoseconds to picoseconds) compared to the oscillation period of the mid-infrared light (several femtoseconds), the electron–phonon and electron–electron scattering times can become much shorter for electrons that are accelerated to high kinetic energies and/or at high densities of excited carriers. As the density of the carriers excited by the control pulse decreases on picosecond time scales, the harmonic signal recovers to the value without the resonant pump after several tens of picoseconds (Peterka et al., 2023).

Using a sub-resonant pump pulse with photon energy lower than the exciton transition energy, the excitons are generated mainly via two-photon absorption driven by a combination of one photon from the control pulse and one photon from the strong infrared driving pulse (Peterka et al., 2023). This process occurs only when the pulses are overlapped in time on the sample. Due to the short duration of pulses used in this study, this leads to ultrafast modulation of HHG at sub-100 fs timescales, thus enabling a new class of fast nonlinear optical devices working in the strong-field regime.

7 Extrinsic HHG enhancement

Enhancing the light-matter interaction by nanostructures is an effective way to increase non-linear effects. A semi-open distributed Bragg reflector can achieve electric field enhancement over the entire area of a TMD monolayer deposited upon it (Liu et al., 2025). Moreover, the semi-open structure prevents the reabsorption of the generated harmonics. When focusing a 2.2-μm femtosecond laser pulse on ML TMDs on the distributed Bragg reflector structure, the third to the seventh order harmonics are enhanced by more than two orders of magnitude compared to MLs on an unstructured substrate (Liu et al., 2025).

8 Conclusion and outlook

The strong light-matter interaction, minimized reabsorption, and intrinsic phase matching make atomically thin semiconductors ideal candidates as active materials in compact EUV light sources, as objects of investigation using HHG, and finally, in novel device concepts based on the modulation of HHG. While very efficient HHG has been demonstrated, the underlying mechanisms are intricate and go beyond the simple three-step model description in many aspects. Further study is required to gain the depth of understanding of aspects like many-body correlation, Berry curvature, and chirality that is necessary to control and optimize HHG. Possible tuning knobs that have in part been already explored are the modulation of the carrier density via ultrafast photodoping (Guan et al., 2020; Wang et al., 2022; Heide et al., 2022; Peterka et al., 2023), chemical doping (Huang et al., 2017; Yu et al., 2019), or electrical gating (Nishidome et al., 2024); and strain (Guan et al., 2019; Bae et al., 2022). The HHG efficiency can be greatly enhanced by distributed Bragg reflectors (Liu et al., 2025) or other semi-opoen resonators such as photonic crystals (Wu et al., 2014), plasmonic nanoantennas (Lee et al., 2015), or the intrinsic optical cavity of tubular analogues of two-dimensional materials (Visic et al., 2019). Furthermore, there is now a whole library of two-dimensional semiconductors far beyond those already tested, and they can be combined into stacks, with the relative angles of their crystal axes as

an additional control parameter (Naik and Jain, 2018; Yuan et al., 2020; Kennes et al., 2021; Ciarrocchi et al., 2022).

Author contributions

CG: Writing – review and editing, Writing – original draft.

Funding

The author(s) declared that financial support was received for this work and/or its publication. This work received funding from the PRIN 2020 project Conquest funded by the Italian Ministry of University and Research (Prot. 2020JZ5N9M).

Conflict of interest

The author(s) declared that this work was conducted in the absence of any commercial or financial relationships that could be construed as a potential conflict of interest.

The handling editor CT declared a past co-authorship with the author CG.

The author CG declared that they were an editorial board member of Frontiers at the time of submission. This had no impact on the peer review process and the final decision.

Generative AI statement

The author(s) declared that generative AI was not used in the creation of this manuscript.

Any alternative text (alt text) provided alongside figures in this article has been generated by Frontiers with the support of artificial intelligence and reasonable efforts have been made to ensure accuracy, including review by the authors wherever possible. If you identify any issues, please contact us.

Publisher's note

References

Antoine, P., L'Huillier, A., and Lewenstein, M. (1996). Attosecond pulse trains using high-order harmonics. *Phys. Rev. Lett.* 77, 1234–1237. doi:10.1103/PhysRevLett.77.1234

Bae, G., Kim, Y., and Lee, J. D. (2022). Revealing berry curvature of the unoccupied band in high harmonic generation. *Phys. Rev. B* 106, 205422. doi:10.1103/PhysRevB.106.205422

Baker, S., Robinson, J. S., Haworth, C. A., Teng, H., Smith, R. A., Chirila, C. C., et al. (2006). Probing proton dynamics in molecules on an attosecond time scale. *Science* 312, 424–427. doi:10.1126/science.1123904

Borzda, T., Gadermaier, C., Vujicic, N., Topolovsek, P., Borovsak, M., Mertelj, T., et al. (2015). Charge photogeneration in few-layer MoS_2. *Adv. Funct. Mater.* 22, 3351–3358. doi:10.1002/adfm.201500709

Bruner, B. D., Masin, Z., Negro, M., Morales, F., Brambilla, D., Devetta, M., et al. (2016). Multidimensional high harmonic spectroscopy of polyatomic molecules: detecting sub-cycle laser-driven hole dynamics upon ionization in strong mid-IR laser fields. *Faraday Discuss.* 194, 369–405. doi:10.1039/C6FD00130K

Calegari, F., Sansone, G., Stagira, S., Vozzi, C., and Nisoli, M. (2007). Advances in attosecond science. *J. Phys. B* 49, 062001. doi:10.1088/0953-4075/49/6/062001

Cao, J., Li, F., Bai, Y., Liu, P., and Li, R. (2021). Inter-half-cycle spectral interference in high-order harmonic generation from monolayer MoS_2. *Opt. Lett.* 29, 4830–4841. doi:10.1364/OE.416213

Chen, Y.-C., Yeh, H., Lee, C.-J., and Chang, W.-H. (2018). Distributed bragg reflectors as broadband and large-area platforms for light-coupling enhancement in 2D transition-metal dichalcogenides. *ACS Appl. Mater. Interfaces* 10, 16874–16880. doi:10.1021/acsami.8b02845

Chernikov, A., Berkelbach, T. C., Hill, H. M., Rigosi, A., Li, Y., Aslan, B., et al. (2014). Exciton binding energy and nonhydrogenic rydberg series in monolayer WS2. *Phys. Rev. Lett.* 113, 076813. doi:10.1103/PhysRevLett.113.076802

Ciarrocchi, A., Tagarelli, F., Avsar, A., and Kis, A. (2022). Excitonic devices with van der Waals heterostructures: valleytronics meets twistronics. *Nat. Rev. Mater.* 7, 449–464. doi:10.1038/s41578-021-00408-7

Corkum, P. B., and Krausz, F. (2007). Attosecond science. *Nat. Phys.* 3, 381–387. doi:10.1038/nphys620

Evans, B. L., and Young, P. A. (1967). Exciton spectra in thin crystals: the diamagnetic effect. *Proc. Phys. Soc.* 91, 475–482. doi:10.1088/0370-1328/91/2/327

Feng, W., Yao, Y., Zhu, W., Zhou, J., Yao, W., and Xiao, D. (2012). Intrinsic spin Hall effect in monolayers of group-VI dichalcogenides: a first-principles study. *Phys. Rev. B* 86, 165108. doi:10.1103/PhysRevB.86.165108

Fontana, M., Deppe, T., Boyd, A. K., Rinzan, M., Liu, A. Y., Paranjape, M., et al. (2013). Electron-hole transport and photovoltaic effect in gated MoS_2 schottky junctions. *Sci. Rep.* 3, 1–6. doi:10.1038/srep01634

Freudenstein, J., Borsch, M., Meierhofer, M., Afanasiev, D., Schmid, C. P., Sandner, F., et al. (2022). Attosecond clocking of correlations between Bloch electrons. *Nature* 610, 290–309. doi:10.1038/s41586-022-05190-2

Garg, M., Kim, H. Y., and Goulielmakis, E. (2018). Ultimate waveform reproducibility of extreme-ultraviolet pulses by high-harmonic generation in quartz. *Nat. Phot.* 12, 291–296. doi:10.1038/s41566-018-0123-6

Ghimire, S., and Reis, D. A. (2019). High-harmonic generation from solids. *Nat. Phys.* 15, 10–16. doi:10.1038/s41567-018-0315-5

Ghimire, S., DiChiara, A. D., Sistrunk, E., Agostini, P., DiMauro, L. F., Reis, D. A., et al. (2011). Observation of high-order harmonic generation in a bulk crystal. *Nat. Phys.* 7, 138–141. doi:10.1038/nphys1847

Golde, D., Meier, T., and Koch, S. W. (2008). High harmonics generated in semiconductor nanostructures by the coupled dynamics of optical inter-and intraband excitations. *Phys. Rev. B* 77, 075330. doi:10.1103/PhysRevB.77.075330

Guan, M.-X., Lian, C., Hu, S.-Q., Liu, H., Zhang, S.-J., Zhang, J., et al. (2019). Cooperative evolution of intraband and interband excitations for high-harmonic generation in strained MoS_2. *Phys. Rev. B* 99, 184306. doi:10.1103/PhysRevB.99.184306

Guan, M., Hu, S., Zhao, H., Lian, C., and Meng, S. (2020). Toward attosecond control of electron dynamics in twodimensional materials. *Appl. Phys. Lett.* 116, 043101. doi:10.1063/1.5135599

Hader, J., Neuhaus, J., Moloney, J. V., and Koch, S. W. (2023). Coulomb enhancement of high harmonic generation in monolayer transition metal dichalcogenides. *Opt. Lett.* 38, 2094–2097. doi:10.1364/OL.485551

He, K., Kumar, N., Zhao, L., Wang, Z., Mak, K. F., Zhao, H., et al. (2014). Tightly bound excitons in monolayer WS_2. *Phys. Rev. Lett.* 113, 026803. doi:10.1103/PhysRevLett.113.026803

Heide, C., Kobayashi, Y., Johnson, A. C., Liu, F., Heinz, T. F., Reis, D. A., et al. (2022). Probing electron-hole coherence in strongly driven 2D materials using high-harmonic generation. *Optica* 9, 512–516. doi:10.1364/OPTICA.444105

Huang, T. F., Zhu, X. S., Li, L., Liu, X., Lan, P. F., and Lu, P. X. (2017). High-order-harmonic generation of a doped semiconductor. *Phys. Rev. A* 96, 043425. doi:10.1103/PhysRevA.96.043425

Jia, L., Zhang, Z., Yang, D. Z., Liu, Y., Si, M. S., Zhang, G. P., et al. (2020). Optical high-order harmonic generation as a structural characterization tool. *Phys. Rev. B* 101, 144304. doi:10.1103/PhysRevB.101.144304

Joensen, P., Frindt, R. F., and Morrison, S. R. (1986). Single-layer MoS2. *Mater. Res. Bull.* 21, 457–461. doi:10.1016/0025-5408(86)90011-5

Kennes, D. M., Claassen, M., Xian, L., Georges, A., Millis, A. J., Hone, J., et al. (2021). Moiré heterostructures as a condensed-matter quantum simulator. *Nat. Phys.* 17, 155–163. doi:10.1038/s41567-020-01154-3

Kobayashi, Y., Heide, C., Kelardeh, H. K., Johnson, A., Liu, F., Heinz, T. F., et al. (2021). Polarization flipping of even-order harmonics in monolayer transition-metal dichalcogenides. *Ultraf. Sci.* 2021, 9820716. doi:10.34133/2021/9820716

Kobayashi, Y., Heide, C., Johnson, A. C., Tiwari, V., Liu, F., Reis, D. A., et al. (2023). Floquet engineering of strongly driven excitons in monolayer tungsten disulfide. *Nat. Phys.* 19, 171–176. doi:10.1038/s41567-022-01849-9

Krausz, F., and Stockman, M. I. (2014). Attosecond metrology: from electron capture to future signal processing. *Nat. Phot.* 8, 205–213. doi:10.1038/nphoton.2014.28

Lanin, A. A., Stepanov, E. A., Fedotov, A. B., and Zheltikov, A. M. (2017). Mapping the electron band structure by intraband high-harmonic generation in solids. *Optica* 4, 516–519. doi:10.1364/OPTICA.4.000516

Lee, B., Park, J., Han, G. H., Ee, H.-S., Naylor, C. H., Liu, W., et al. (2015). Fano resonance and spectrally modified photoluminescence enhancement in monolayer MoS_2 integrated with Plasmonic Nanoantenna array. *Nano Lett.* 15, 3646–3653. doi:10.1021/acs.nanolett.5b01563

Lee, V. C., Yue, L., Gaarde, M. B., Chan, Y.-H., and Qiu, D. Y. (2024). Many-body enhancement of high-harmonic generation in monolayer MoS_2. *Nat. Commun.* 15, 6228. doi:10.1038/s41467-024-50534-3

Li, J., Lu, J., Chew, A., Han, S., Li, J., Wu, Y., et al. (2020). Attosecond science based on high harmonic generation from gases and solids. *Nat. Commun.* 11, 2748. doi:10.1038/s41467-020-16480-6

Liu, H., Li, Y., You, Y. S., Ghimire, S., Heinz, T. F., and Reis, D. A. (2017). High-harmonic generation from an atomically thin semiconductor. *Nat. Phys.* 13, 262–266. doi:10.1038/nphys3946

Liu, C., Zheng, Y., Zeng, Z., and Li, R. (2020). Polarization-resolved analysis of high-order harmonic generation in monolayer MoS_2. *New J. Phys.* 22, 073046. doi:10.1088/1367-2630/ab9a88

Liu, X., Li, W., He, W., Qiao, S., Guan, C., Liang, S., et al. (2025). Enhancement of high-harmonic generation from 2D materials by distributed Bragg reflector. *Appl. Phys. Lett.* 126, 191101. doi:10.1063/5.0266306

Lou, Z., Zheng, Y., Liu, C., Zhang, L., Ge, X., Li, Y., et al. (2020). Ellipticity dependence of nonperturbative harmonic generation in few-layer MoS_2. *Opt. Commun.* 469, 125769. doi:10.1016/j.optcom.2020.125769

Luu, T. T., Garg, M., Kruchinin, S.Yu, Moulet, A., Hassan, M.Th., and Goulielmakis, E. (2015). Extreme ultraviolet high-harmonic spectroscopy of solids. *Nature* 521, 498–502. doi:10.1038/nature14456

Naik, M. H., and Jain, M. (2018). Ultraflatbands and shear solitons in moiré patterns of twisted bilayer transition metal dichalcogenides. *Phys. Rev. Lett.* 121, 266401. doi:10.1103/PhysRevLett.121.266401

Nishidome, H., Omoto, M., Nagai, K., Uchida, K., Murakami, Y., Eda, J., et al. (2024). Influence of laser intensity and location of the fermi level on tunneling processes for high-harmonic generation in arrayed semiconducting carbon nanotubes. *ACS Photonics* 11, 171–179. doi:10.1021/acsphotonics.3c01244

Peng, R., Liang, L., Hood, Z. D., Boulesbaa, A., Puretzky, A., Ievlev, A. V., et al. (2016). In-Plane heterojunctions enable multiphasic two-dimensional (2D) MoS_2 nanosheets as efficient photocatalysts for hydrogen evolution from water reduction. *ACS Catal.* 6, 6723–6729. doi:10.1021/acscatal.6b02076

Peterka, P., Slobodeniuk, A. O., Novotny, T., Suthar, P., Bartos, M., Trojanek, F., et al. (2023). High harmonic generation in monolayer MoS_2 controlled by resonant and near-resonant pulses on ultrashort time scales. *Apl. Photonics* 8, 086103. doi:10.1063/5.0158995

Sandoval, J. S., Yang, D., Frindt, R. F., and Irwin, J. C. (1991). Raman study and lattice dynamics of single molecular layers of MoS_2. *Phys. Rev. B* 44, 3955–3962. doi:10.1103/PhysRevB.44.3955

Sansone, G., Benedetti, E., Calegari, F., Vozzi, C., Avaldi, L., Flammini, R., et al. (2006). Isolated single-cycle attosecond pulses. *Science* 314, 443–446. doi:10.1126/science.1132838

Schaibley, J. R., Yu, H., Clark, G., Rivera, P., Ross, J. S., Seiler, K. L., et al. (2016). Valleytronics in 2D materials. *Nat. Revs. Mater* 1, 1–15. doi:10.1038/natrevmats.2016.55

Schiffrin, A., Paasch-Colberg, T., Karpowicz, N., Apalkov, V., Gerster, D., Muhlbradt, S., et al. (2013). Optical-field-induced current in dielectrics. *Nature* 493, 70–74. doi:10.1038/nature11567

Schubert, O., Hohenleutner, M., Langer, F., Urbanek, B., Lange, C., Huttner, U., et al. (2014). Sub-cycle control of terahertz high harmonic generation by dynamical Bloch oscillations. *Nat. Photonics* 8, 119–123. doi:10.1038/NPHOTON.2013.349

Schultze, M., Bothschafter, E. M., Sommer, A., Holzner, S., Schweinberger, W., Fiess, M., et al. (2013). Controlling dielectrics with the electric field of light. *Nature* 493, 75–78. doi:10.1038/nature11720

Silva, R. E. F., Blinov, I. V., Rubtsov, A. N., Smirnova, O., and Ivanov, M. (2018). High-harmonic spectroscopy of ultrafast many-body dynamics in strongly correlated systems. *Nat. Phot.* 12, 266–270. doi:10.1038/s41566-018-0129-0

Smirnova, O., Mairesse, Y., Patchkovskii, S., Dudovich, N., Villeneuve, D., Corkum, P., et al. (2009). High harmonic interferometry of multi-electron dynamics in molecules. *Nature* 460, 972–977. doi:10.1038/nature08253

Trovatello, C., Marini, A., Xu, X., Lee, C., Liu, F., Curreli, N., et al. (2021). Optical parametric amplification by monolayer transition metal dichalcogenides. *Nat. Phot.* 15, 6–10. doi:10.1038/s41566-020-00728-0

Trovatello, C., Katsch, F., Li, Q., Zhu, X., Knorr, A., Cerullo, G., et al. (2022). Disentangling many-body effects in the coherent optical response of 2D semiconductors. *Nano Lett.* 22 (13), 5322–5329. doi:10.1021/acs.nanolett.2c01309

Vampa, G., McDonald, C. R., Orlando, G., Klug, D. D., Corkum, P. B., and Brabec, T. (2014). Theoretical analysis of high-harmonic generation in solids. *Phys. Rev. Lett.* 113, 073901. doi:10.1103/PhysRevLett.113.073901

Vampa, G., Hammond, T. J., Thire, N., Schmidt, B. E., Legare, F., McDonald, C. R., et al. (2015a). All-Optical reconstruction of Crystal band structure. *Phys. Rev. Lett.* 115, 193603. doi:10.1103/PhysRevLett.115.193603

Vampa, G., Hammond, T., Thire, N., Schmidt, B., Legare, F., McDonald, C., et al. (2015b). Linking high harmonics from gases and solids. *Nature* 522, 462–464. doi:10.1038/nature14517

Vega-Mayoral, V., Vella, D., Borzda, T., Prijatelj, M., Tempra, I., Pogna, E. A. A., et al. (2016). Exciton and charge carrier dynamics in few-layer WS_2. *Nanoscale* 8, 5428–5434. doi:10.1039/c5nr08384b

Vella, D., Ovchinnikov, D., Martino, N., Vega-Mayoral, V., Dumcenco, D., Kung, Y.-C., et al. (2017). Unconventional electroabsorption in monolayer MoS_2. *2D Mater.* 4, 021005. doi:10.1088/2053-1583/aa5784

Visic, B., Yadgarov, L., Pogna, E. A. A., Dal Conte, S., Vega-Mayoral, V., Vella, D., et al. (2019). Ultrafast nonequilibrium dynamics of strongly coupled resonances in the intrinsic cavity of WS_2 nanotubes. *Phys. Rev. Res.* 1, 033046. doi:10.1103/PhysRevResearch.1.033046

Vozzi, C., Cirmi, G., Manzoni, C., Benedetti, E., Calegari, F., Sansone, G., et al. (2006). High-energy, few-optical-cycle pulses at 1.5 μm with passive carrier-envelope phase stabilization. *Opt. Expr.* 14, 10109–10116. doi:10.1364/OE.14.010109

Vozzi, C., Calegari, F., Benedetti, E., Gasilov, S., Sansone, G., Cerullo, G., et al. (2007). Millijoule-level phase-stabilized few-optical-cycle infrared parametric source. *Opt. Lett.* 32, 2957–2959. doi:10.1364/OL.32.002957

Vozzi, C., Negro, M., Calegari, F., Sansone, G., Nisoli, M., De Silvestri, S., et al. (2011). Generalized molecular orbital tomography. *Nat. Phys.* 7, 822–826. doi:10.1038/nphys2029

Wang, Y., Iyikanat, F., Bai, X., Hu, X., Das, S., Dai, Y., et al. (2022). Optical control of high-harmonic generation at the atomic thickness. *Nano Lett.* 22, 8455–8462. doi:10.1021/acs.nanolett.2c02711

Wu, S., Buckley, S., Jones, A. M., Ross, J. S., Ghimire, N. J., Yan, J., et al. (2014). Control of two-dimensional excitonic light emission *via* photonic crystal. *2D Mater.* 1, 011001. doi:10.1088/2053-1583/1/1/011001

Wu, M., Ghimire, S., Reis, D. A., Schafer, K. J., and Gaarde, M. B. (2015). High-harmonic generation from bloch electrons in solids. *Phys. Rev. A* 91, 043839. doi:10.1103/PhysRevA.91.043839

Xiao, D., Liu, G. B., Feng, W., Xu, X., and Yao, W. (2012). Coupled spin and valley physics in monolayers of MoS_2 and other group-VI dichalcogenides. *Phys. Rev. Lett.* 108, 196802. doi:10.1103/PhysRevLett.108.196802

Ye, Y., Wong, Z. J., Lu, X., Ni, X., Zhu, H., Chen, X., et al. (2015). Monolayer excitonic laser. *Nat. Phot.* 9, 733–737. doi:10.1038/nphoton.2015.197

Yin, Z., Li, H., Li, H., Jiang, L., Shi, Y., Sun, Y., et al. (2012). Single-layer MoS_2 phototransistors. *ACS Nano* 6, 74–80. doi:10.1021/nn2024557

Yoshikawa, N., Nagai, K., Uchida, K., Takaguchi, Y., Sasaki, S., Miyata, Y., et al. (2019). Interband resonant high-harmonic generation by valley polarized electron–hole pairs. *Nat. Commun.* 10, 3709. doi:10.1038/s41467-019-11697-6

Yu, C., Hansen, K. K., and Madsen, L. B. (2019). Enhanced high-order harmonic generation in donor-doped band-gap materials. *Phys. Reb. A* 99, 013435. doi:10.1103/PhysRevA.99.013435

Yuan, L., Zheng, B. Y., Kunstmann, J., Brumme, T., Kuc, A. B., Ma, C., et al. (2020). Twist-angle-dependent exciton diffusion in WS_2-WSe_2 heterobilayers. *Nat. Mater.* 19, 617–623. doi:10.1038/s41563-020-0670-3

Yue, L., Hollinger, R., Uzundal, C. B., Nebgen, B., Gan, Z., Nadjafidehaghani, E., et al. (2022). Signatures of multiband effects in high-harmonic generation in monolayer MoS_2. *Phys. Rev. Lett.* 129, 147401. doi:10.1103/PhysRevLett.129.147401

Zhang, H., Lu, S. B., Zheng, J., Du, J., Wen, S. C., Tang, D. Y., et al. (2014). Molybdenum disulfide (MoS_2) as a broadband saturable absorber for ultra-fast photonics. *Opt. Express* 22, 7249–7260. doi:10.1364/OE.22.007249